NANO LETTERS

Letter

pubs.acs.org/NanoLett

High-Efficiency Selective Electron Tunnelling in a Heterostructure Photovoltaic Diode

Chuancheng Jia,[†] Wei Ma,[‡,§] Chunhui Gu,[†] Hongliang Chen,[†] Haomiao Yu,[∥] Xinxi Li,[†] Fan Zhang,[‡,§] Lin Gu,[‡,§] Andong Xia,[⊥] Xiaoyuan Hou,[∥] Sheng Meng,[*,‡,§] and Xuefeng Guo[*,†,#]

[†]Center for Nanochemistry, Beijing National Laboratory for Molecular Sciences, State Key Laboratory for Structural Chemistry of Unstable and Stable Species, College of Chemistry and Molecular Engineering, Peking University, Beijing 100871, China

[‡]Institute of Physics and Beijing National Laboratory for Condensed Matter Physics, Chinese Academy of Sciences, Beijing 100190, China

[§]Collaborative Innovation Center of Quantum Matter, Beijing, 100190, China

[∥]Department of Physics, Fudan University, Shanghai 200433, China

[⊥]Institute of Chemistry, Chinese Academy of Sciences, Beijing 100190, China

[#]Department of Materials Science and Engineering, College of Engineering, Peking University, Beijing 100871, China

S *Supporting Information*

ABSTRACT: A heterostructure photovoltaic diode featuring an all-solid-state TiO_2/graphene/dye ternary interface with high-efficiency photogenerated charge separation/transport is described here. Light absorption is accomplished by dye molecules deposited on the outside surface of graphene as photoreceptors to produce photoexcited electron−hole pairs. Unlike conventional photovoltaic conversion, in this heterostructure both photoexcited electrons and holes tunnel along the same direction into graphene, but only electrons display efficient ballistic transport toward the TiO_2 transport layer, thus leading to effective photon-to-electricity conversion. On the basis of this ipsilateral selective electron tunnelling (ISET) mechanism, a model monolayer photovoltaic device (PVD) possessing a TiO_2/graphene/acridine orange ternary interface showed ∼86.8% interfacial separation/collection efficiency, which guaranteed an ultrahigh absorbed photon-to-current efficiency (APCE, ∼80%). Such an ISET-based PVD may become a fundamental device architecture for photovoltaic solar cells, photoelectric detectors, and other novel optoelectronic applications with obvious advantages, such as high efficiency, easy fabrication, scalability, and universal availability of cost-effective materials.

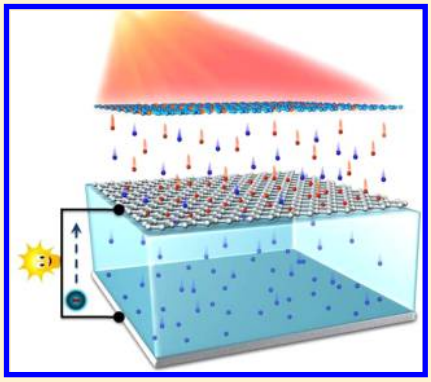

KEYWORDS: *Graphene, photovoltaics, interface, electron tunnelling*

Photodiode, which is composed of homo- or heterosemiconductor structures or metal−semiconductor heterostructures is the fundamental structure for photovoltaic solar cells, photoelectric detectors, and other functional optoelectronic devices.[1,2] In all these photodiode-based devices, especially photovoltaic devices, electron−hole pairs are created by light absorption in a semiconductor layer, and the positive and negative charges are separated/transported in opposite directions at the heterojunction interfaces with electron/hole selective conductor layers and electron/hole collecting electrodes on each side of the semiconductor layer.[3,4] To boost the development of this field, simple and reliable interface designs for high-efficiency photogenerated charge separation/transport are urgently needed to enable developing low-cost photovoltaic and optoelectronic device architectures featuring high efficiency.[5,6] In this work, we demonstrate a distinct heterostructure photovoltaic diode with an all-solid-state ternary interface that consists of a TiO_2 electron collection thin film, single-layer graphene (SLG), and a monolayer of dye molecules (a TiO_2/SLG/dye ternary interface). Unlike conventional photovoltaic conversion, in this photovoltaic device (PVD) both photoexcited electrons and holes tunnel along the same direction into graphene, but only electrons display high-efficiency ballistic transport toward the TiO_2 transport layer. This ipsilateral selective electron tunnelling (ISET) mechanism leads to an ultrahigh absorbed photon-to-current efficiency (APCE, ∼80%). Such an ISET-based PVD may become a fundamental device architecture for photovoltaic solar cells, photoelectric detectors, and other novel optoelectronic applications.[7,8]

Graphene, a two-dimensional (2D) crystalline monolayer made of sp^2-bonded carbon atoms arranged in a honeycomb lattice, has been widely used as an electrode materials for efficient charge collection in a wide variety of optoelectronic devices including dye-sensitized solar cells (DSSCs),[9] photo-

Received: February 19, 2016
Revised: May 7, 2016
Published: May 16, 2016

DOI: 10.1021/acs.nanolett.6b00727
Nano Lett. 2016, 16, 3600−3606

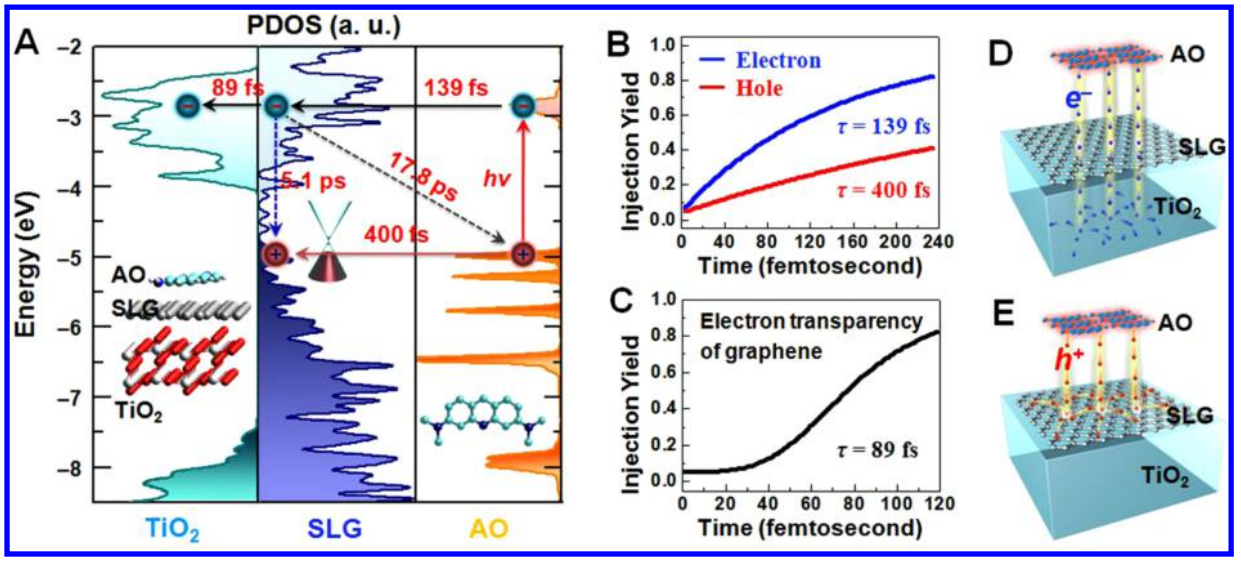

Figure 1. ISET mechanism at the TiO_2/SLG/AO ternary interface. (A) PDOS spectra for TiO_2, SLG, and AO showing that the unique interfacial electronic structure leads to ipsilateral separation of the photogenerated carriers and selective ballistic electron tunnelling across graphene to the TiO_2 layer. The insets show a ball-and-stick model for the layered structure of the ternary interface (left) and the molecular structure of the AO dye (right) (Figure S1). (B) Comparison of electron and hole injection dynamics at the SLG/AO interface. Electrons migrate into graphene within a time scale of ~139 fs (blue line representing single exponential fitting; for original data, see Figure S3A). Holes migrate into graphene within a time scale of ~400 fs (red line representing single exponential fitting; for original data, see Figure S3A). (C) Electron emission dynamics with an injection time of ~89 fs at the TiO_2/SLG interface (Figure S3B). (D,E) Schematic representation of direct ballistic tunnelling of the photogenerated electrons across graphene toward TiO_2 (D) and photogenerated hole collection at the graphene layer (E).

detectors,[10] and organic/molecular electronic devices,[11] because of its high carrier mobility, high mechanical flexibility, and environmental stability. Another remarkable feature of graphene is its one-atom thickness, which confers it with photon and electron transparency. Particularly, electron transparency makes graphene behave like a noble metal,[12] allowing electrons with very low-energy (<3 eV) to ballistically transport through graphene with high efficiency.[13] In combination with our previous work, where we demonstrated that either electrons or holes or both can be transferred from photoactive materials to graphene,[14,15] these unique features strongly imply that electrons and holes may behave differently after simultaneously tunnelling into graphene, potentially facilitating charge separation and enabling photovoltaic applications.

To explore this potential, we designed a model system with a TiO_2/SLG/acridine orange (AO) ternary interface, where AO dye molecules serving as photoreceptors were deposited on the external surface of the TiO_2/SLG Schottky diode. Figure 1A shows the electronic band structure of the TiO_2/SLG/AO ternary interface (Figure S1 in the Supporting Information). On the basis of the projected density of states (PDOS) spectra calculated by density functional theory (DFT), we found that the lowest unoccupied molecular orbit (LUMO) of AO lying at about −2.7 eV relative to the vacuum level well matches the unoccupied electronic states of the adjacent graphene layer, which are then strongly coupled to the conduction band (CB) states of the TiO_2. Similarly, the highest occupied molecular orbit (HOMO) of AO at about −5.0 eV matches the occupied states of graphene. We have also calculated the contributions from atomic orbitals to the PDOS of the system as shown in Figure S2. The conduction band minimum of the rutile TiO_2 substrate (~−4.0 eV) results from the Ti 3d electrons, whereas the valence band maximum of TiO_2 (~−7.3 eV) basically originates from the 2p electrons of O atoms. It is apparent that the 2p electrons of C atoms make major contributions to the PDOS of graphene. In the similar way, C 2p electrons and N 2p electrons form the energy bands of the AO sensitizer from −8.5 to −2 eV. The important difference is that this HOMO energy level of the AO lies well within the energy band gap of TiO_2. Therefore, we predict that the similarity in the band alignment at the AO/SLG interface could allow both electrons and holes to ipsilaterally migrate toward graphene, while the difference with respect to TiO_2 electronic states might selectively drive electrons, rather than holes, to ballistically tunnel to and over the Schottky barrier, thus efficiently completing the charge separation process. This hypothesis is first proved by the theoretical real-time simulations of the interfacial dynamic charge transfer processes using nonadiabatic molecular dynamics within the time-dependent density functional theory (TDDFT) framework as discussed below.

On the basis of real-time TDDFT simulations, the photogenerated electron at the AO LUMO and the hole at the AO HOMO can be injected from AO to graphene but with a different injection lifetimes (τ) (~139 fs for the electron and ~400 fs for the hole) (Figure 1B and Figure S3A). More importantly, only the injected electron can further tunnel into the conduction band of TiO_2 with an injection lifetime of ~89 fs (Figure 1C and Figure S3B) owing to the well-matched interfacial electronic states. The injected holes remain staying in the graphene. In addition, the injected electron's energy relaxation and recombination processes (Figure 1A and Figures S4 and S5) have time scales of τ_{rel} = ~5.1 ps and τ_{rec} = ~17.8 ps, respectively, much slower than that of electron tunnelling (τ_{tun} = ~89 fs). Then, the electron collection efficiency can be calculated according to the formula $(1/\tau_{tun})/(1/\tau_{rel} + 1/\tau_{rec} + 1/\tau_{tun})$, which affords a value of 97.8%, a harbinger for the high photon-to-current conversion efficiency described below. Note that the recombination lifetime we obtained here is the averaged result of two separate trajectories (Figure S6), which

DOI: 10.1021/acs.nanolett.6b00727
Nano Lett. 2016, 16, 3600−3606

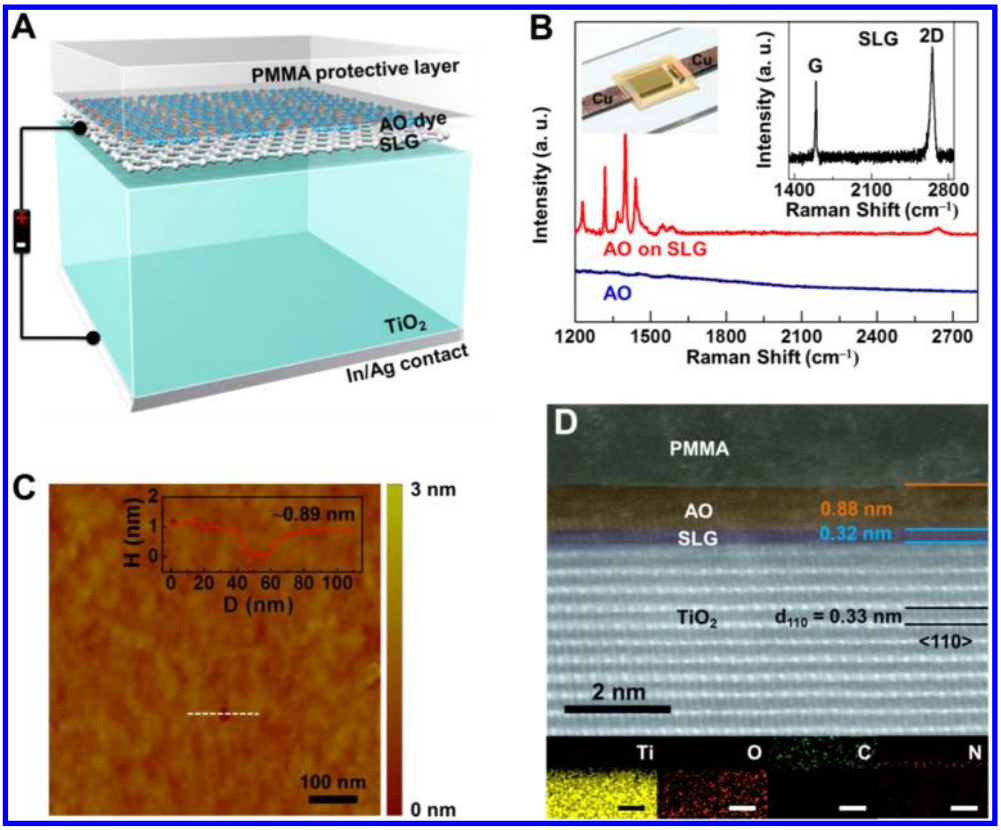

Figure 2. Device structure. (A) Schematic of the designed TiO_2/SLG/AO ternary interface device structure. (B) Raman spectra of pure AO on silicon substrates (blue) and AO after assembly on graphene (red). The left inset shows an optical image of a real device, where the In/Ag contact and graphene were connected by copper to the external electrical circuit. The right inset shows the Raman spectrum of the high-quality CVD-grown SLGs. (C) Surface morphology of the TiO_2/SLG/AO ternary interface, demonstrating the formation of a uniform high-coverage AO monolayer with 0.89 ± 0.11 nm thickness, obtained from a selected defect. (D) Cross-sectional high-resolution dark-field STEM image of the TiO_2/SLG/AO ternary interface with a PMMA protective layer. The insets show the titanium, oxygen, carbon, and nitrogen elemental compositions of individual layers (all scale bars are 2 nm).

correspond to excited electrons transferred to different energy states of graphene CB. All these final states are low energy degenerate states of graphene CB and do not represent the substantial physical differences. The two separate trajectories gave the almost identical recombination lifetime, 15.3 and 18.3 ps, respectively, therefore the averaged value of 17.8 ps is a reasonable estimate for the recombination lifetime between graphene CB and HOMO of AO. Consequently, similar to electron tunnelling transport in a single-molecule device,[16] the photoexcited electrons of AO have a surprising ballistic transport across graphene toward TiO_2 without any energy loss (Figure 1D).[13] This selective electron emission at the ternary interfaces can be used to realize ipsilateral charge separation/transport (Figures 1D,E). After charge separation, TiO_2 acts as an electron collecting electrode, while graphene serves as a good hole conductor.

To prove the mechanism's effectiveness, we fabricated a model monolayer photovoltaic device with the designed TiO_2/SLG/AO ternary interface. A schematic of the whole device structure is shown in Figure 2A. The device fabrication process is detailed in the Supporting Information. In brief, rutile TiO_2 (001) single crystals with atomically flat surfaces, confirmed by AFM and HRTEM characterizations (Figure S7), were used as a wide bandgap semiconductor layer for electron collection; 100 nm In/100 nm Ag were thermally evaporated onto the back side to produce ohmic metal back contacts. Single-layer graphene was grown by a low-pressure chemical vapor deposition (LPCVD) method under optimal conditions[17] and was transferred onto the TiO_2 surface using an isopropanol-assisted dry-transfer method, which guarantees that there are no water molecules or other residues trapped at the TiO_2/SLG interface. Such a dry-transfer method realizes good contact between TiO_2 and graphene and avoids the disturbance of water molecules or other residues to the photogenerated electron tunnelling across the TiO_2/SLG interface and carrier transport in the SLG layer. In the Raman spectrum (Figure 2B, right inset), the narrow single symmetric 2D peak (~2650 cm^{-1}), small G/2D ratio, and negligible D peak indicate that the obtained graphene was single-layer and of high quality,[18] which is also evidenced by its light absorption of 2.7−2.9% (Figure S8A).[19] Next, AO molecules were thermally evaporated onto the graphene surface followed by annealing at 140 °C to ensure a uniform and compact molecular arrangement. Figure 2C shows a high-resolution AFM image taken after AO assembly, confirming the formation of a uniform high-coverage AO monolayer with an approximately 0.89 nm thickness. From the surface-enhanced Raman spectra shown in Figure 2B, enhanced Raman signals of AO at the wavelengths from 1200 to 1600 cm^{-1} on the graphene substrates were observed owing to fluorescence quenching by graphene, indicating that the AO molecules, which have a π-conjugated flat structure, were in intimate contact with graphene. On the top of the AO monolayer was a layer of poly(methyl methacrylate) (PMMA), which was used as a supporting layer during graphene transfer

DOI: 10.1021/acs.nanolett.6b00727
Nano Lett. 2016, 16, 3600−3606

and a protective layer for the device. The almost 99% light transmittance of the PMMA layer indicates that it had negligible effect on light absorption of the device (Figure S8B).

Cross-sectional scanning transmission electron microscopy (STEM) revealed the layered structure of the TiO_2/SLG/AO ternary interface (Figure 2D and Figure S9). As shown in Figure 2D, the distinct lattice structure of a rutile TiO_2 (001) single crystal with interface spacing of ~0.33 nm in the ⟨110⟩ direction and an atomically sharp surface was observed (also see Figure S7). On the TiO_2 surface was a single atomic layer graphene with an ~0.32 nm thickness; on the graphene surface was a uniform monolayer of AO with thickness of ~0.88 nm, consistent with AFM characterizations (Figure 2C). To clearly image the subtle interfacial structure, the elemental compositions of the individual layers were analyzed using energy-dispersive X-ray spectroscopy (EDX). The presence of N shown in the inset of Figure 2D, which is the fingerprint of AO molecules in the monolayer, confirms the layered structure of the TiO_2/SLG/AO ternary interface. In combination with X-ray photoelectron spectroscopic (XPS) studies (Figure S10), all the Raman, AFM, and STEM results indicated that an intimately contacting layer-by-layer TiO_2/SLG/AO ternary interface had been established at the atomic level, thus ensuring the success of the following photovoltaic applications.

Figure 3A illustrates how a TiO_2/SLG/AO device works. The AO dye molecules absorb light and generate electron−hole pairs. The photoactivated electrons tunnel through graphene to the TiO_2 layer and then transport to the back electrode with Ohmic contacts for collection, while the photoactivated holes are transferred to the graphene layer for collection. With the back metal electrode as a photoanode and graphene as a photocathode, connected together externally to form a circuit, the photoelectric conversion is finally achieved. Figure 3B shows the current−voltage characteristics of a working device with a TiO_2/SLG/AO ternary interface and a control device with a TiO_2/SLG binary interface measured in the dark and under visible light (>420 nm) illumination (P_{in} = 100 mW cm^{-2}). Under illumination, the working device exhibited an open-circuit photovoltage (V_{OC}) of ~0.608 V, a short circuit current density (J_{SC}) of ~8.84 μA cm^{-2} and a fill factor (FF) of ~0.4139. In traditional photovoltaic devices, the open-circuit photovoltage is determined by the energy level difference between the electron collection electrode and the hole collection electrode. For the TiO_2/SLG/AO device, the conduction band (E_{CB}) of the TiO_2 electron collection electrode is at about −4.1 eV and the Fermi level (E_F) of the SLG hole collection electrode is at about −4.7 eV as shown in Figure 1A. The experimental value of V_{OC} (~0.608 V) is consistent with the energy level difference (~0.6 V) between E_{CB} of TiO_2 and E_F of SLG. In addition, with gradually increasing the thickness of the AO dye layer from ~0.88 to ~12.0 nm the J_{SC} of the devices increases from ~8.84 to ~16.78 μA cm^{-2} (Figure S11). This can be attributed to the enhanced absorption of the AO layer, especially for the AO dye adjacent to the TiO_2/SLG/AO ternary interface within the distance of ~3 nm. However, V_{OC} and FF of the devices have a slight decrease with increasing the thickness of the AO layer. This is due to the influence on the Fermi level of SLG by photoexcited AO with different thicknesses, thus changing V_{OC} and FF of the devices.[15] The control device without the AO dye showed nearly negligible photocurrent response, confirming that the photoresponse of the TiO_2/SLG/AO device mainly originated from the photoexcited AO monolayer, not from either of the photoinduced electron−hole pairs in the graphene[20] or the photoexcitation of the TiO_2 substrate (Figure S12). In addition, the current−voltage curves measured in the dark for both the TiO_2/SLG/AO and the control device exhibited similar rectifying characteristics. This observation demonstrates that a Schottky contact was formed at the TiO_2/SLG interface and that the assembled AO dye had little effect on the Schottky barrier of the heterojunction.

To further confirm the origin of the observed photoresponse, the incident photon-to-current conversion efficiency (IPCE) of

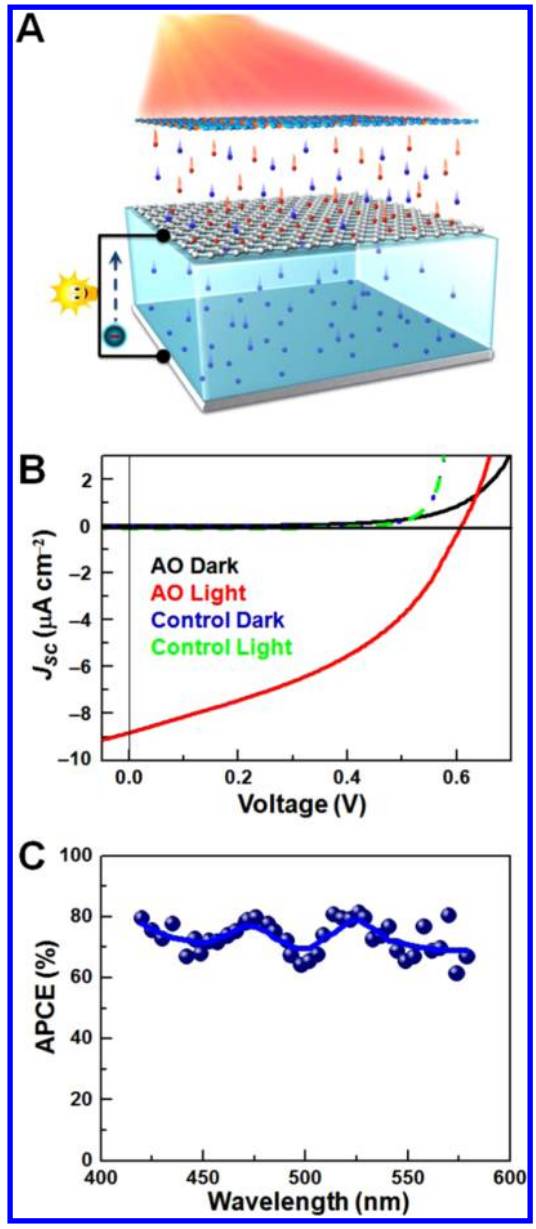

Figure 3. Photovoltaic energy conversion characteristics. (A) Schematic illustration of the mechanism of the photovoltaic effect. Blue and red globules represent electrons and holes, respectively. (B) Current−voltage characteristics of the device measured in the dark (AO Dark, black solid line) and under 100 mW cm^{-2} visible (>420 nm) illumination (AO Light, red solid line). For comparison, a control device without the AO dye was also studied in the dark (Control Dark, blue dashed line) and under the same illumination conditions (Control Light, bright green dashed line). (C) APCE spectrum derived from the IPCE and the LHE spectra, demonstrating an ultrahigh internal quantum efficiency of ~80%.

DOI: 10.1021/acs.nanolett.6b00727
Nano Lett. 2016, 16, 3600−3606

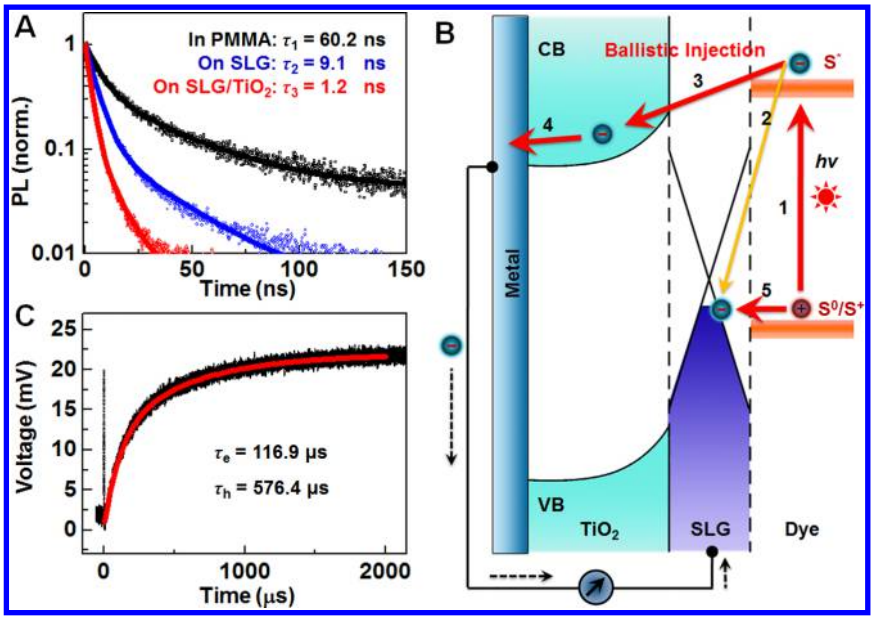

Figure 4. Interfacial charge separation/transport dynamics. (A) Normalized time-resolved photoluminescence (PL) decay traces measured at 535 nm for the AO dye dispersed in PMMA matrix (black), assembled on suspended graphene (blue), and assembled on a TiO_2/SLG binary interface (red) after excitation at 473 nm. The dominant PL decay time (τ) constants are summarized in Table S1. (B) Schematic of the general dynamic processes of charge separation and transport in a photovoltaic device with a TiO_2/SLG/dye ternary interface. The thick red arrows indicate the processes desirable for energy conversion. (*hv*, photoexcitation). (C) Transient photovoltage measurements. Light pulses were supplied by the 532 nm line of an Nd:YAG laser. The data were fitted to a double exponential curve (red line). The sudden jump at the moment of laser turn-on may have been caused from some unknown negligible interfacial effect in the device.[30]

the device was measured as a function of excitation wavelength (Figure S13), which is directly related to the short-circuit current under corresponding monochromatic light illumination. The absorption spectrum of a parallel AO sample, an identical SLG/AO/PMMA film on quartz substrates (Figure S14), was measured simultaneously. This allowed the light harvesting efficiency (LHE) of the AO monolayer to be determined from its absorption spectrum. As shown in Figure S13, both the IPCE spectrum of the device and the LHE spectrum of the AO monolayer share the similar shape and the approximate maximum peaks in the 420−580 nm spectral range, again demonstrating that the photocurrent of the devices was caused by the contribution of the AO dye.

Another important feature of merit for PVDs is the absorbed photon-to-current efficiency (APCE), which reflects the intrinsic quantum efficiency of photogenerated charge separation at the interface. This can be calculated by dividing the device IPCE by the LHE of the AO monolayer (APCE (%) = IPCE (%)/LHE (%)). From the APCE spectrum of the TiO_2/SLG/AO device (Figure 3C), we achieved an extraordinary internal quantum efficiency of 65−80%. Also, a maximum value of ∼80% is obtained at two peaks of 475 and 525 nm, which originates from the effective separation and transfer of the hole−electron pairs generated at these peak ranges. Thereinto, the large noise for APCE at the wavelength range from 530 to 580 nm is due to the low absorption of AO at the tail, which leads to the small values for IPCE and LHE and thus large random errors for APCE (IPCE/LHE). This is significant, considering the fact that the photovoltaic energy conversion in our devices occurs from only a 0.89 nm thick AO monolayer. In addition, in comparison with control devices with a TiO_2/AO/SLG ternary structure (Figure S15), the internal quantum efficiency of the TiO_2/SLG/AO device is as high as that of control devices with conventional photon-to-current conversion mechanisms. However, with similar thickness of the AO layer the V_{OC} in TiO_2/SLG/AO devices (∼0.608 V) is much larger than that in control TiO_2/AO/SLG devices (∼0.447 V). To prove the reliability and reproducibility of this technique, we performed the same measurements after replacing the AO molecules with another typical dye, Z907. The obtained TiO_2/SLG/Z907 ternary interface-based devices displayed the following consistent results: an open-circuit photovoltage of ∼580 mV, a short-circuit current density of ∼6.46 μA cm^{-2}, and an APCE of ∼60% under 100 mW cm^{-2} visible light (>420 nm) illumination (Figures S16 and S17). Therefore, like traditional PVDs,[21,22] the present device structure produces efficient charge separation and transport. Its advantage lies in that it is a simple multilayer with electron/hole separation and collection integrated into one side of a bilayer Schottky junction, thus making cost-effective all-solid-state photovoltaic solar cells with a simplified device structure and easy fabrication technologies.[23]

The competition between the charge separation/collection processes and the recombination loss processes of the photogenerated electron−hole pairs determines the photoelectric conversion efficiency of PVDs.[24] To further understand the ipsilateral separation mechanism taking place at the TiO_2/SLG/dye ternary interface, the charge-transfer dynamic processes of the TiO_2/SLG/AO device were studied by transient photoluminescence (PL)[25] and transient photovoltage methods.[26] Before studying the intrinsic lifetimes (τ) of the dye's excited states, AO molecules were dispersed in the PMMA matrix and measured by a PL method. On the basis of the PL decay profile of the AO dye (black in Figure 4A), the dominant PL decay time (τ_1) was calculated by data fitting to be ∼60.2 ns (Table S1), which corresponds to the intrinsic interband recombination rate of the AO excitons. When AO was assembled onto the surface of suspended graphene, the

DOI: 10.1021/acs.nanolett.6b00727
Nano Lett. 2016, 16, 3600−3606

recombination rate had a dominant PL decay time (τ_2) of ~9.1 ns (blue in Figure 4A), a significant decrease that should be attributed to the transfer of excited electrons from AO to graphene (Process 2 in Figure 4B). For the TiO_2/SLG/AO sample, the dominant PL decay time (τ_3) was further reduced to ~1.2 ns (red in Figure 4A). This was caused by the faster electron tunnelling from AO across graphene to TiO_2 (Process 3 in Figure 4B). Because the efficiency of interfacial photogenerated charge carrier separation is determined by the competition between effective charge transfer and inefficient loss processes, the interfacial separation efficiency can be calculated according to the formula $(1/\tau_3)/(1/\tau_1 + 1/\tau_2 + 1/\tau_3)$, which affords a value of ~86.8%. This value agrees surprisingly well with the APCE spectrum of the TiO_2/SLG/AO device (Figure 3C).

The transient photovoltage rise has a quantitative relationship with the dynamic processes of charge transport in PVDs.[26] The photovoltage generation processes occurring in the TiO_2/SLG/AO device were equivalent to the charging processes of the In−Ag/TiO_2/SLG parallel-plate capacitor in which the In/Ag back metal layer and the graphene layer are regarded as the two electrodes of the capacitor sandwiching an intermediate TiO_2 dielectric layer. As shown in Figure 4C, the transient photovoltage rise times for the TiO_2/SLG/AO device with ~0.88 nm AO after excitation with a 532 nm pulse laser are well fitted to a double exponential curve as follows: $V = 21.98 - 10.24 \times \exp(-t/576.4) - 11.18 \times \exp(-t/116.9)$ with a mean square error of 0.9663, where V is the value of the transient photovoltage in unit of millivolts and t is the responding time in unit of microsecond. Considering the charging processes in the In−Ag/TiO_2/SLG capacitor and the results from the control TiO_2/SLG/AO device with ~6.0 nm AO (Figure S18), the faster rise time constant of ~116.9 μs is attributed to the dye thickness-independent process of photogenerated electron injection and transport on the conduction band of the TiO_2 layer to the In/Ag back metal electrode (Process 4 in Figure 4B); the slower rise time constant of ~576.4 μs corresponds to the dye thickness-dependent process of hole injection into the hole-collecting graphene layer (Process 5 in Figure 4B). Additionally, from the transient photovoltage decay spectrum of the device, the recombination rate of the injected electrons on the TiO_2 conduction band with the injected holes on the graphene was calculated to have a time scale of ~35.1 ms (Figure S19),[27] which is much slower than the effective charge separation process. Therefore, on the basis of the above transient photoluminescence and transient photovoltage results, we conclude that the effective photogenerated charge separation and collection processes in our devices are much faster than the noneffective recombination and back transfer processes, thus producing the high-efficiency photoelectric conversion. The major dynamic processes of charge separation and transport in our TiO_2/SLG/dye ternary interface-based devices are schematically illustrated in Figure 4B.

The work demonstrated here presented a new conceptual and technological platform for achieving all-solid-state and high-efficiency photovoltaic conversion. By taking advantage of the electron transparency of graphene and the internal ballistic electron emission, we have developed a PVD model system featuring a sophisticated TiO_2/SLG/dye ternary interface. Unlike traditional photovoltaic conversion, these devices, based on an ISET-based mechanism, demonstrate high internal quantum efficiency of up to ~80%. With such high internal quantum efficiency, ISET-based PVDs may become a fundamental device architecture for practical photovoltaic solar cells and photoelectric detectors by comprehensively considering the following factors: (1) Interface engineering for optimizing the energy alignment at the critical interface.[28] The donor/acceptor levels of the excited dye, the Fermi level of the middle conductor, and the positions of the semiconductor conduction/valence bands should meet the energy level relationship shown in Figure 4B. (2) The barrier height and the ballistic electron emission rate, which are related to the physical and electronic coupling of the photoreceptors to the semiconductors for efficient charge separation and transport. (3) The key ways for achieving the performance breakthrough are to maximize light harvesting and minimize energy loss by the careful choice of device materials with long excited state lifetimes, high carrier mobilities and suitable thickness,[22,29] and the use of light-trapping strategies.[21] To achieve cheap large-area solar cells, alternative organic semiconductors are needed instead of inorganic semiconductors such as TiO_2 and ZnO. This will allow the fabrication of solution-processed, foldable devices on flexible substrates or the construction of a p-type Schottky diode that induces hot hole ballistic injection. Consequently, these photovoltaic and photoelectric applications are expected with obvious advantages, such as high efficiency, easy fabrication, scalability, and universal availability of cost-effective materials. In addition to these, this ISET mechanism and corresponding photodiode structure promise the design and fabrication of a new generation of multifunctional interfaces, ultrasensitive sensors, and optoelectronic devices.

■ ASSOCIATED CONTENT

Supporting Information

The Supporting Information is available free of charge on the ACS Publications website at DOI: 10.1021/acs.nanolett.6b00727.

Details of device fabrication and characterization, theoretical calculation, Figures S1−S19, and Table S1. (PDF)

■ AUTHOR INFORMATION

Corresponding Authors

*E-mail: guoxf@pku.edu.cn (X.G.).
*E-mail: smeng@iphy.ac.cn (S.M.).

Author Contributions

C.J. and W.M. contributed equally to this work.

Funding

This work was supported by the National Natural Science Funds of China (21225311, 91333102, 21373014, and 11222431) and the 973 Project (2012CB921404 and 2012CB921403).

Notes

The authors declare no competing financial interest.

■ REFERENCES

(1) Anderson, B.; Anderson, R. *Fundamentals of Semiconductor devices*; McGraw-Hill, Inc.: New York, 2004.

(2) Sze, S. M.; Ng, K. K. *Physics of semiconductor devices*; John Wiley & Sons: New York, 2006.

(3) Wurfel, P. *Physics of Solar Cells: From Basic Principles to Advanced Concepts*; Wiley-VCH: Weinheim, Germany, 2005.

(4) Britnell, L.; Ribeiro, R. M.; Eckmann, A.; Jalil, R.; Belle, B. D.; Mishchenko, A.; Kim, Y. J.; Gorbachev, R. V.; Georgiou, T.; Morozov,

DOI: 10.1021/acs.nanolett.6b00727
Nano Lett. 2016, 16, 3600−3606

S. V.; Grigorenko, A. N.; Geim, A. K.; Casiraghi, C.; Castro Neto, A. H.; Novoselov, K. S. *Science* **2013**, *340*, 1311−1314.
(5) Zhou, H.; Chen, Q.; Li, G.; Luo, S.; Song, T. b.; Duan, H. S.; Hong, Z.; You, J.; Liu, Y.; Yang, Y. *Science* **2014**, *345*, 542−546.
(6) Sambur, J. B.; Novet, T.; Parkinson, B. A. *Science* **2010**, *330*, 63−66.
(7) Yu, W. J.; Liu, Y.; Zhou, H. L.; Yin, A. X.; Li, Z.; Huang, Y.; Duan, X. F. *Nat. Nanotechnol.* **2013**, *8*, 952−958.
(8) Sarkar, D.; Xie, X.; Liu, W.; Cao, W.; Kang, J.; Gong, Y.; Kraemer, S.; Ajayan, P. M.; Banerjee, K. *Nature* **2015**, *526*, 91−95.
(9) Roy-Mayhew, J. D.; Aksay, I. A. *Chem. Rev.* **2014**, *114*, 6323−6348.
(10) Koppens, F. H. L.; Mueller, T.; Avouris, P.; Ferrari, A. C.; Vitiello, M. S.; Polini, M. *Nat. Nanotechnol.* **2014**, *9*, 780−793.
(11) Cao, Y.; Dong, S.; Liu, S.; He, L.; Gan, L.; Yu, X.; Steigerwald, M. L.; Wu, X.; Liu, Z.; Guo, X. *Angew. Chem., Int. Ed.* **2012**, *51*, 12228−12232.
(12) Seah, M.; Dench, W. *Surf. Interface Anal.* **1979**, *1*, 2−11.
(13) Srisonphan, S.; Kim, M.; Kim, H. K. *Sci. Rep.* **2014**, *4*, 3764.
(14) Zhang, D.; Gan, L.; Cao, Y.; Wang, Q.; Qi, L.; Guo, X. *Adv. Mater.* **2012**, *24*, 2715−2720.
(15) Jia, C.; Li, H.; Jiang, J.; Wang, J.; Chen, H.; Cao, D.; Stoddart, J. F.; Guo, X. *Adv. Mater.* **2013**, *25*, 6752−6759.
(16) Jia, C.; Guo, X. *Chem. Soc. Rev.* **2013**, *42*, 5642−5660.
(17) Jia, C.; Jiang, J.; Gan, L.; Guo, X. *Sci. Rep.* **2012**, *2*, 707.
(18) Ferrari, A. C.; Meyer, J. C.; Scardaci, V.; Casiraghi, C.; Lazzeri, M.; Mauri, F.; Piscanec, S.; Jiang, D.; Novoselov, K. S.; Roth, S.; Geim, A. K. *Phys. Rev. Lett.* **2006**, *97*, 187401.
(19) Bonaccorso, F.; Sun, Z.; Hasan, T.; Ferrari, A. C. *Nat. Photonics* **2010**, *4*, 611−622.
(20) Long, R.; English, N. J.; Prezhdo, O. V. *J. Am. Chem. Soc.* **2012**, *134*, 14238−14248.
(21) Sargent, E. H. *Nat. Photonics* **2012**, *6*, 133−135.
(22) Habas, S. E.; Platt, H. A. S.; van Hest, M.; Ginley, D. S. *Chem. Rev.* **2010**, *110*, 6571−6594.
(23) McFarland, E. W.; Tang, J. *Nature* **2003**, *421*, 616−618.
(24) Hodes, G. *J. Phys. Chem. C* **2008**, *112*, 17778−17787.
(25) Haque, S. A.; Palomares, E.; Cho, B. M.; Green, A. N. M.; Hirata, N.; Klug, D. R.; Durrant, J. R. *J. Am. Chem. Soc.* **2005**, *127*, 3456−3462.
(26) Chen, X.; Wu, B. *Rev. Sci. Instrum.* **2015**, *86*, 013905.
(27) Walker, A. B.; Peter, L. M.; Lobato, K.; Cameron, P. J. *J. Phys. Chem. B* **2006**, *110*, 25504−25507.
(28) Grätzel, M. *Nature* **2001**, *414*, 338−344.
(29) Stranks, S. D.; Snaith, H. J. *Nat. Nanotechnol.* **2015**, *10*, 391−402.
(30) Mahrov, B.; Boschloo, G.; Hagfeldt, A.; Dloczik, L.; Dittrich, T. *Appl. Phys. Lett.* **2004**, *84*, 5455−5457.

DOI: 10.1021/acs.nanolett.6b00727
Nano Lett. 2016, 16, 3600−3606